

Choice of Interceptor Aerodynamic Lifting Surface Location based on Autopilot Design Considerations

R.B. Sankar^{#,*}, P. K. Tiwari[#], B. Bandyopadhyay[@], and H. Arya[@]

[#]DRDO-Defence Research and Development Laboratory, Hyderabad - 500 058, India

[@]Indian Institute of Technology Bombay, Mumbai - 400 076, India

^{*}E-mail: rambankar@gmail.com

ABSTRACT

Interceptors operate at wide range of operating conditions in terms of Mach number, altitude and angle of attack. The aerodynamic design caters for such wide operating envelope by appropriate sizing of lifting and control surfaces for meeting the normal acceleration capability requirements. The wide range of operating conditions leads to an inevitable spread in center of pressure location and hence spread in static stability. The performance of control design is a strong function of the aerodynamic static stability. The total operating envelope can be bifurcated into statically stable and unstable zones and the aerodynamic lifting surface location can be used as a control parameter to identify the neutral stability point. During the homing phase lesser static stability is desirable for good speed of response, hence the lifting surface location needs to be chosen based on the capability of control to handle instability. This paper analyses the limitations of autopilot design for the control of an unstable interceptor and brings out a method to identify the optimum aerodynamic lifting surface location for efficiently managing static margin while satisfying the control limitations and homing phase performance. This provides an input on the most appropriate lifting surface location to the aerodynamic designer during the initial CFD based aerodynamic characterisation stage itself, before commencing the rigorous wind tunnel based characterisation.

Keywords: Interceptor; Aerodynamic static stability; Autopilot; Stability margins; Aerodynamic lifting surface

NOMENCLATURE

α	Angle of Attack (rad)	I_{yy}	Interceptor moment of inertia ($kg\cdot m^2$)
ΔC_m	Control moment coefficient $f(M, \alpha, \delta)$	K_α	OL gain of the three-loop autopilot
ΔC_N	Control force coefficient $f(M, \alpha, \delta)$	K_b	DC gain of control deflection to body rate plant transfer function
δ	Tail control deflection (rad)	K_{dc}	DC gain of the three-loop autopilot
ω_{af}	Airframe natural frequency (rad/s)	K_q	IML gain of the three-loop autopilot
ω_{ap}	Desired second order non-dominant pole natural frequency of closed loop transfer function (rad/s)	K_z	DC gain of control deflection to normal acceleration plant transfer function
ω_l	IL gain of the three-loop autopilot	$N(s)$	Numerator of desired closed loop transfer function
ω_z	Location of zeros in control deflection to normal acceleration plant transfer function (rad/s)	T_α	Turning rate time constant (s)
ζ_{af}	Airframe damping ratio	T_{ap}	Desired first order dominant pole time constant of closed loop transfer function (s)
ζ_{ap}	Desired second order non-dominant pole damping ratio of closed loop transfer function	V_m	Interceptor velocity (m/s)
a_z	Normal acceleration (usually referred as latax for an interceptor) (m/s^2)	D	Reference length (m)
a_{ZC}	Commanded normal acceleration (m/s^2)	IL	Inner loop of the three-loop autopilot
$C_{m\alpha}$	C_m linearised slope w.r.t. α at an operating point $(\partial C_m / \partial \alpha)(rad^{-1})$	IML	Inner-most loop of the three-loop autopilot
$C_{m\delta}$	C_m linearised slope w.r.t. δ at an operating point $(\partial C_m / \partial \delta)(rad^{-1})$	M	Interceptor Mach number
C_m	Pitching moment coefficient $f(M, \alpha)$	m	Interceptor mass (kg)
$C_{N\alpha}$	C_N linearised slope w.r.t. α at an operating point $(\partial C_N / \partial \alpha)(rad^{-1})$	OL	Outer loop of the three-loop autopilot
$C_{N\delta}$	C_N linearised slope w.r.t. δ at an operating point $(\partial C_N / \partial \delta)(rad^{-1})$	Q	Dynamic pressure (N/m^2)
C_N	Normal force coefficient $f(M, \alpha)$	q	Body rate (rad/s)
		S	Reference area (m^2)

1. INTRODUCTION

The role of an interceptor control designer begins right from the configuration design itself. The broad requirements for an interceptor are posed in terms of range, target interception altitudes and target envelope which need to be translated into interceptor configuration. Interceptor configuration design and

sizing is an iterative exercise mainly between the propulsion, aerodynamic, structures and control and simulation teams with constraints imposed by the avionics. The target characteristics, range requirement and ground system define the avionics like seeker, data link and INS which acts like a constraint in interceptor sizing exercise. Platform limitations pose another constraint on interceptor length, weight and diameter.

The target definition and kill envelope defines requirement on latability capability and aerodynamic time constants of the interceptor. The aerodynamic designer sizes the aerodynamic surfaces satisfying this requirement considering the operating point in terms of Mach and altitude, thus generating drag of the configuration. However, the drag leads to change in Mach number which is the start of an iterative process to converge on propulsion, weight and aerodynamics to bring out a baseline configuration.

The baseline configuration is the starting point for control design exercise as it provides the first set of aerodynamic data in terms of drag data (C_D), normal force coefficient data, moment characteristics (C_m) and control characteristics. The aerodynamic lifting surface design freezes the spread of the static margin across the operating envelope as a function of Mach number and angle of attack (AoA). However, the positioning of the lifting surface along the length of the interceptor can be used as a control parameter to decide the point of neutral stability in static margin spread; depending upon the capability to handle instability. The static stability varies from stable to unstable regions at various operating points and the static instability is represented in terms of right half s-plane pole in control sense. Unstable plants put constraints on control design¹. Given the actuator bandwidth constraints owing to hinge moment and power limitations, there exists a maximum unstable pole level which can be stabilised in closed loop with good robustness (in terms of stability margins). The lifting surface location is a parameter that is decided by the aerodynamic designer based on the maximum instability the autopilot can handle, while satisfying the trim requirements. Thus the maximum instability that can be handled dictates the position of lifting surface location to complete the second level of aerodynamic design.

Nesline explains the methodology for arriving at the bounds on some aerodynamic parameters from an autopilot design perspective². In this work we bring out the level of unstable pole which can be handled for given actuator leading to choice of the lifting surface location to minimise the static margin in homing phase, which is a first of its kind work to the best of author's knowledge. In this work we also propose a method to enhance the unstable pole handling capability by the autopilot. This paper uses a conventional three-loop autopilot³ design for all the analysis.

Three-loop autopilot has been a very commonly used design method for controlling interceptor latability channel over the years. The work presented in this paper uses the conventional three-loop autopilot design technique for controlling unstable interceptors. This section tries to address various autopilot design approaches reported in the literature.

Mracek examines all the possible three-loop topologies for autopilot to bring out the best in terms of robustness⁴. Nesline

presents an autopilot design approach that combines classical and modern control based design to obtain performance at high and low frequencies respectively⁵. Nesline explains the importance of aerodynamic parameters consideration in autopilot design exercise². Nesline demonstrates the importance of analysing the modern control design techniques in the classical control based frequency response analysis in terms of gain crossover frequency to ascertain the stability⁶. Defu addresses the non-minimum phase behaviour associated with a tail-controlled missile⁷. It also compares the stabilisation of unstable missiles using two-loop and three-loop topologies, and further proposes addition of PI controller to improve the performance of classical three-loop topology.

Hai-rong proposes a three-loop autopilot design gain tuning methodology as function of various flight parameters⁸. Mracek shows the gain scheduling techniques for the design of three channel roll, pitch and yaw autopilots with three-loop topology⁹. Li explores applying three-loop autopilot to spinning missiles¹⁰. Abd-elatif addresses the optimisation of three-loop autopilot gains under crossover frequency constraints using numerical optimisation based gain adjustment technique¹¹.

Devaud demonstrates the autopilot design using linear and non-linear control design techniques¹². Lee establishes the connection between linear and non-linear autopilots with three-loop topology and it is shown that both are identical from control signal perspective¹³. A three-loop autopilot augmented with H_∞ optimisation was designed for controlling highly unstable missiles¹⁴.

The work presented in this paper brings out a first of its kind methodology to identify the optimum aerodynamic lifting surface location for efficiently managing static margin while satisfying the control limitations and homing phase performance. The proposed methodology is arrived through analysis of limitations posed by autopilot design in controlling a statically unstable interceptor. The analysis is carried out using a conventional classical control based three-loop autopilot technique, which is widely used in industries.

2. MODELLING A TAIL CONTROL INTERCEPTOR

A hypothetical interceptor configuration is considered for all the analysis in this paper with fixed lifting surfaces and movable tail control surfaces. For latability autopilot design the plant of interest is the relation of tail control deflection with the pitch-yaw channel accelerations and body rates. The plant is linearised at an operating point (M, α) to obtain linearised aerodynamic coefficient slopes ($C_{N\alpha}, C_{m\alpha}$) and control effectiveness slopes ($C_{N\delta}, C_{m\delta}$) to obtain the transfer functions. The transfer function representation³ of the pitch-yaw channel dynamics is obtained as follows.

$$\frac{a_z(s)}{\delta(s)} = \frac{K_z \left(1 - \frac{s^2}{\omega_z^2}\right)}{\frac{s^2}{\omega_{af}^2} + \frac{2\zeta_{af}}{\omega_{af}}s + 1} \quad (1)$$

$$\frac{q(s)}{\delta(s)} = \frac{K_b (1 + T_\alpha s)}{\frac{s^2}{\omega_{af}^2} + \frac{2\zeta_{af}}{\omega_{af}}s + 1}$$

$$K_z = -V_m \frac{M_\alpha Z_\delta - Z_\alpha M_\delta}{M_\alpha} \quad K_b = \frac{K_z}{V_m}$$

where

$$\omega_z = \sqrt{\frac{M_\alpha Z_\delta - Z_\alpha M_\delta}{Z_\delta}} \quad \omega_{af} = \sqrt{-M_\alpha} \quad (2)$$

$$T_\alpha = \frac{M_\delta}{M_\alpha Z_\delta - Z_\alpha M_\delta} \quad \zeta_{af} = \frac{Z_\alpha \omega_{af}}{2M_\alpha}$$

$$M_\alpha = \frac{QSD}{I_{yy}} C_{m\alpha} \quad M_\delta = \frac{QSD}{I_{yy}} C_{m\delta} \quad (3)$$

$$Z_\alpha = -\frac{QS}{mV_m} C_{N\alpha} \quad Z_\delta = -\frac{QS}{mV_m} C_{N\delta}$$

One of the important parameters of an interceptor latrix channel is static stability signified by a variable known as static margin given by

$$h = -\frac{C_{m\alpha}}{C_{N\alpha}} \quad (4)$$

Positive static margin which also means negative pitching moment coefficient slope with respect to AoA ($C_{m\alpha} < 0$) signifies static stability. Similarly, negative static margin which also means positive pitching moment coefficient slope with respect to AoA ($C_{m\alpha} > 0$) signifies static instability. $C_{m\alpha}$ and hence static margin strongly depends on the choice of lifting surface location and also on the flight parameters Mach number and AoA. From a control perspective when the interceptor is statically unstable, it can be better represented as unstable pole which is the right hand side s-plane pole location of the transfer function shown in Eqn (1) given by

$$\omega_{unstable} = \sqrt{M_\alpha} = \sqrt{\frac{QSD}{I_{yy}} C_{m\alpha}} \quad (5)$$

For a given lifting surface location; the stability, instability and their levels strongly depend on the interceptor flight parameters – Mach No and AoA – as shown in Fig. 1. As mentioned earlier it can be seen that the static margin variation across the operating envelope is quite high. Though the extent of static margin spread cannot be avoided, the lifting surface location can decide the neutral stability operating zone (which means zero static margin - as shown in Fig. 1). Hence depending on the maximum instability that can be handled from the control perspective, the aerodynamic designer has a choice of positioning the lifting surface location along the length of the interceptor. After initial few seconds from the launch, the interceptor operates at supersonic Mach numbers. During this phase; as the Mach number increases, the center of pressure (CP) location moves forward and the stability degrades. Hence at high Mach numbers (propulsion boost-end phase) maximum static instability is observed. The homing phase of the interceptor is typically characterised by medium Mach numbers and high AoA in order to intercept maneuvering targets. During homing phase, the interceptor configuration is statically stable. It is desirable to have low static margin during the homing phase² for good speed of response. For the same spread of static margin; if more static instability can be handled

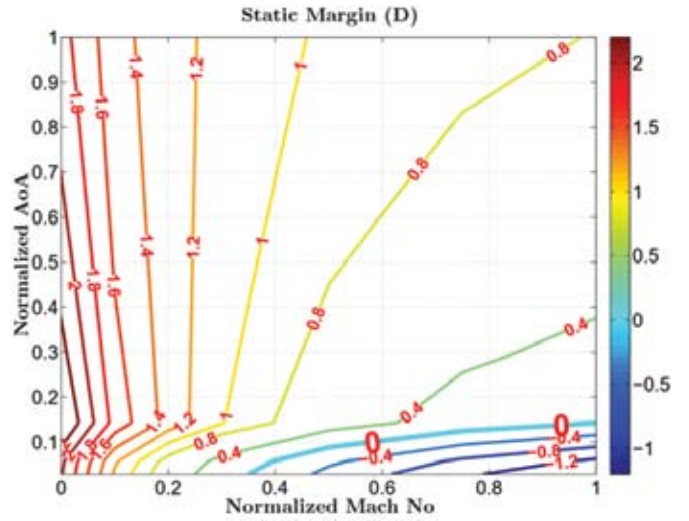


Figure 1. Static margin.

at high Mach number, lower static margin can be obtained in homing phase by suitable placement of lifting surface. This is illustrated as follows.

The aerodynamic designer provides the bounds on feasible lifting surface location along the length of the interceptor, that satisfies the trim requirements meeting the maximum latrix. Let us assume the static margin variation for a nominal lifting surface location be as shown in Fig. 1. The maximum static instability is seen to be $-1.2D$ at high Mach number and low AoA combination. At the homing phase of the interceptor characterised by medium Mach numbers (0.4-0.6 in Fig. 1) and high AoA (0.7-1.0 in Fig. 1), the static margin is seen to be around $+1.0D$. The movement of lifting surface along the length of interceptor changes the value of static margin; but is assumed to maintain the spread pattern of it, which is almost true.

Suppose the lifting surface is moved rearward by a distance such that the maximum instability reduces from $-1.2D$ to $-0.8D$ ($+0.4D$) as shown in Fig. 2. This results in increase of static stability in homing phase of the interceptor to $+1.4D$, which is undesirable as mentioned earlier.

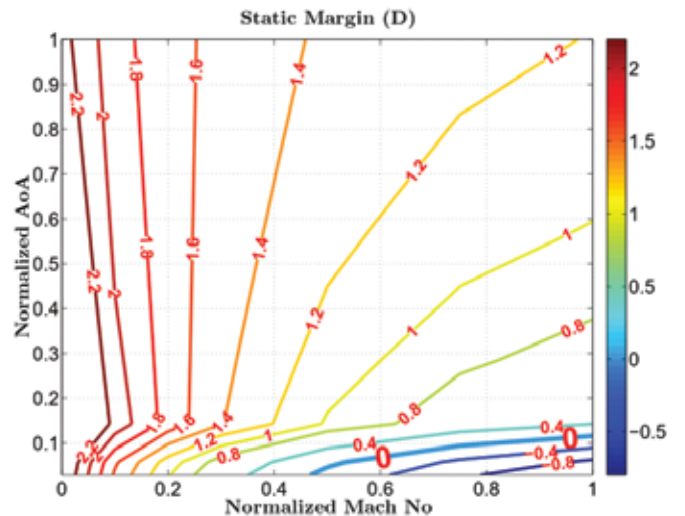


Figure 2. Static margin - lifting surface moved rearward.

On the other hand suppose the lifting surface is moved forward by a distance such that the homing phase static stability reduces from +1.0D to +0.6D (-0.4D) as shown in Fig. 3. This results in increase in static instability at high Mach number and low AoA combination of the interceptor to -1.6D. The feasibility of having such high static instability configuration depends on the capability of control design to handle the resultant open loop unstable pole with good relative stability.

The subsequent sections focus on bringing out the maximum aerodynamic instability that can be handled by the control design with a given actuator in order to obtain the optimum lifting surface location.

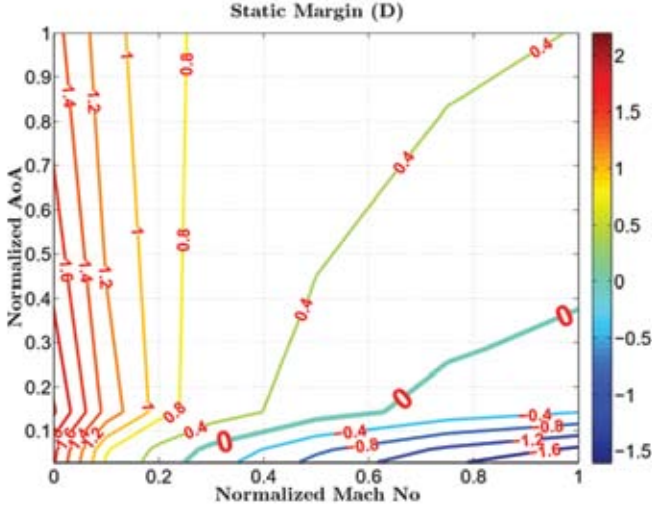


Figure 3. Static margin - lifting surface moved forward.

3. DESIGN OF THREE-LOOP AUTOPILOT FOR LATAX CONTROL

3.1 Algorithmic Approach

A conventional and commonly used three-loop autopilot³ is applied to stabilise and track the latak command. The three-loop autopilot structure is as shown in Fig. 4. The three loops are the Outer loop (OL), Inner loop (IL) and Inner-most loop (IML). The outer loop is an acceleration control loop, whereas the inner loop with pure integrator is a synthetic stability loop. The inner-most loop is a body rate control loop^{3,2}.

The desired closed loop transfer function shown in Eqn (6) is compared against the actual closed loop transfer function obtained from Fig. 4 and the equations for computing the gains in the three-loop autopilot can be obtained.

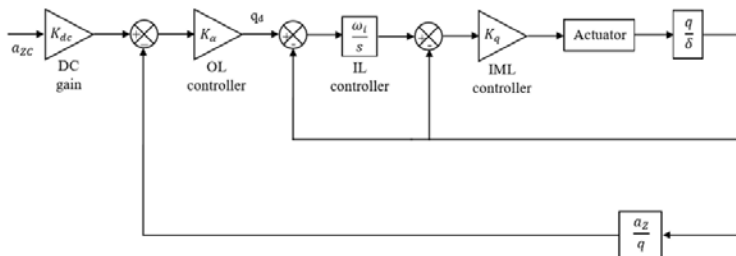


Figure 4. Three-loop autopilot structure.

$$\frac{a_z}{a_{zc}} = \frac{N(s)}{(1 + sT_{ap}) \left(1 + \frac{2\zeta_{ap}}{\omega_{ap}} s + \frac{s^2}{\omega_{ap}^2} \right)} \quad (6)$$

Since the plant shown in Fig. 4 is a strong function of flight parameters (Mach number, AoA and Dynamic Pressure), the desired closed loop transfer function parameters ($T_{ap}, \zeta_{ap}, \omega_{ap}$) are also scheduled as a function of these flight parameters in the autopilot design.

The conventional three-loop autopilot gives good amount of robustness through tuning of desired closed loop transfer function algorithmically. However, the level of plant instability that can be handled with good robustness in terms of stability margins with a given actuator needs to be evaluated. There must be a spectral separation in the three loops of the autopilot. The inner-most loop being the fastest among the three loops usually exhibits least stability margins. In view of computing the least stability margins among the three loops, the open loop transfer function is evaluated analytically with the inner-most loop open. For the sake of simplicity the sensor models are ignored.

Define the plant transfer functions as

$$\frac{q}{\delta} = \frac{q_{num}}{P(s)} \quad \frac{a_z}{\delta} = \frac{a_{znum}}{P(s)} \quad (7)$$

where

$P(s)$ - Plant characteristic polynomial

Define the actuator transfer function as

$$TF_{act} = \frac{A_{num}}{A_{den}} \quad (8)$$

Through block diagram manipulations the open loop transfer function can be obtained as shown in Eqn (9).

$$IML_{open} = \frac{G_1 G_2}{P(s)}$$

$$G_1 = \frac{K_q \omega_i}{s} \left(1 + \frac{s}{\omega_i} \right) \frac{A_{num}}{A_{den}} \quad (9)$$

$$G_2 = a_{znum} \frac{K_\alpha}{\left(1 + \frac{s}{\omega_i} \right)} + q_{num}$$

The open loop transfer function will turn out to be as shown in Eqn (10).

$$IML_{open} = \frac{b_0 s^3 + b_1 s^2 + b_2 s + b_3}{a_0 s^3 + a_1 s^2 + a_2 s + a_3} \frac{1}{P(s)} \quad (10)$$

where

b, a - Coefficients of transfer function $G_1 G_2$

$P(s)$ - Plant characteristic polynomial (typically second order)

The airframe damping ratio of an interceptor is generally small and is usually neglected. Also, plant is considered to be unstable with one unstable pole for all the analysis in this paper. Hence the plant characteristic polynomial is chosen as $P(s) = s^2 - p^2$.

where

p - Location of plant transfer function poles $s = \pm p$

The plant is assumed to have one stable pole located at $s = -p$ and one unstable pole located at $s = p$. The objective is to compute the maximum unstable pole with which the autopilot can guarantee good relative stability specified by again margin of 6 dB and a phase margin of 30 deg with the given actuator dynamics. The stability margins have to be computed as follows.

At phase crossover frequency ω_{pc} , the phase angle of open loop transfer function shown in Eqn (10) implies

$$\begin{aligned} \angle IML_{open} = -\pi \Rightarrow \\ \tan^{-1} \left[\frac{-b_0 \omega_{pc}^3 + b_2 \omega_{pc}}{-b_1 \omega_{pc}^2 + b_3} \right] \\ - \tan^{-1} \left[\frac{-a_0 \omega_{pc}^3 + a_2 \omega_{pc}}{-a_1 \omega_{pc}^2 + a_3} \right] \\ - \tan^{-1} \left[\frac{0}{-\omega_{pc}^2 - p^2} \right] = -\pi \end{aligned} \quad (11)$$

In order to satisfy a gain margin of 6 dB, the magnitude $|IML_{open}|$ must be 0.5 at phase crossover frequency, ω_{pc} ; which implies

$$\begin{aligned} \sqrt{\frac{(-b_0 \omega_{pc}^3 + b_2 \omega_{pc})^2 + (-b_1 \omega_{pc}^2 + b_3)^2}{(-a_0 \omega_{pc}^3 + a_2 \omega_{pc})^2 + (-a_1 \omega_{pc}^2 + a_3)^2}} \\ \times \frac{1}{-\omega_{pc}^2 - p^2} = 0.5 \end{aligned} \quad (12)$$

The phase crossover frequency ω_{pc} has to be represented in terms of pole location p from the phase Eqn (11) and needs to be substituted into magnitude Eqn (12) to solve for the pole location p . Then the phase margin needs to be checked whether it meets the specifications.

However, the analytical solution is difficult as it can be seen that Eqns (11) and (12) involves third order expressions and inverse tangent functions. Hence to bring out the maximum unstable pole satisfying relative stability requirements, we need to resort to an iterative method.

3.2 Iterative Approach

As explained in the previous section, it is difficult to analytically bring out the maximum instability level with which the relative stability requirements can be ensured with a given actuator. Hence the algorithmic approach for autopilot design is

overlooked and an iterative search simulation-based approach is adopted to achieve the same result, which is elaborated in this section. The three autopilot gains (K_α, ω_i and K_q) are iterated in steps within a range of values. In addition to these gains, the plant pole location is also iterated by varying the lifting surface location along the length of the interceptor. The parameters which are iterated are marked in red in Fig. 5.

There are bounds on the three autopilot gains within which the characteristic equation of the actual closed loop transfer function (with plant and autopilot only) as shown in Eqn (13)³ will have poles on the left half of the s-plane.

$$\frac{a_z}{a_{zc}} = \frac{N(s)}{1 + D_1 s + D_2 s^2 + D_3 s^3} \quad (13)$$

where

$$\begin{aligned} D_1 &= \left(\frac{2\zeta_0}{\omega_0} - \frac{1}{K_0} \right) \\ D_2 &= \left(\frac{1}{\omega_0^2} - \frac{2\zeta_{af}}{\omega_{af} K_0} \right) \end{aligned} \quad (14)$$

$$D_3 = -\frac{1}{\omega_{af}^2 K_0}$$

and

$$\begin{aligned} K_0 &= K_q \omega_i K_\alpha \left(\frac{K_b}{K_\alpha} + K_z \right) \\ \frac{2\zeta_0}{\omega_0} &= \frac{K_b (1 + \omega_i T_\alpha)}{\omega_i (K_b + K_\alpha K_z)} \\ \frac{1}{\omega_0^2} &= \frac{\left(K_b T_\alpha - \frac{K_\alpha \omega_i K_z}{\omega_z^2} \right)}{\omega_i (K_b + K_\alpha K_z)} \end{aligned} \quad (15)$$

The characteristic equation of desired closed loop transfer function is

$$1 + D_1 s + D_2 s^2 + D_3 s^3 = 0 \quad (16)$$

The combination of three-loop autopilot gains (K_α, ω_i and K_q) satisfying Routh's necessary and sufficient conditions shown in Eqn (17) leads to absolute stability of the closed loop system.

$$\begin{aligned} D_1 > 0 \quad D_2 > 0 \quad D_3 > 0 \\ D_3 > 0 \quad D_2 > 0 \quad \frac{D_2 D_1 - D_3}{D_2} > 0 \end{aligned} \quad (17)$$

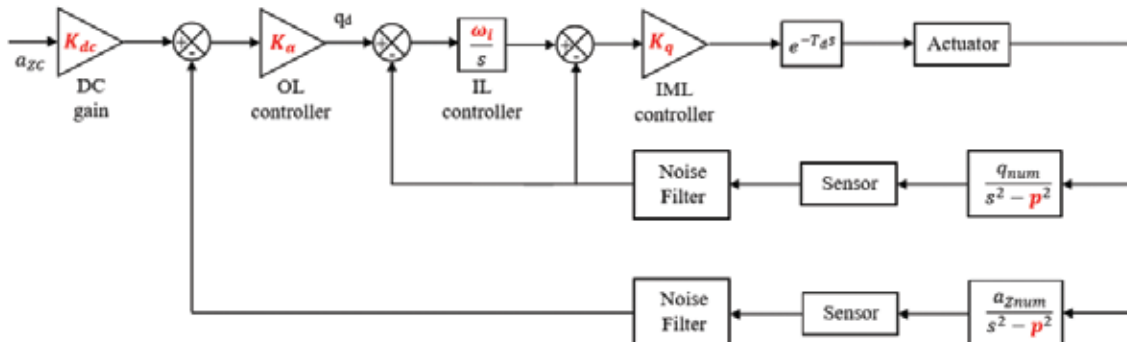


Figure 5. Iteration of three-loop autopilot gains.

For this combination of gains which satisfies Routh’s stability criterion, stability margins for all the three loops are evaluated. The plant perturbations on control effectiveness are also considered while evaluating the stability margins. The maximum unstable pole with which the relative stability requirements are satisfied for any combination of three-loop gains is obtained through this simulation procedure. The interceptor typically exhibits maximum unstable pole at peak Mach number and low AoA as shown earlier in Fig. 1. Hence the simulation procedure explained in this section is carried out at this single operating point only, to arrive at the most appropriate lifting surface location. The design is subsequently verified to ensure stability margins at other operating points. It is seen that with the actuator considered (Bandwidth = 25 Hz, Damping ratio = 0.6), the maximum unstable pole which could give a relative stability of Gain Margin > 6 dB, Phase Margin > 30 deg for all the three loops is 10 rad/s.

This is illustrated in Fig. 6 using contour plots, which shows the variation of stability margins (minimum among all the three loops) as a function of control gain as the unstable pole increases. At lower unstable pole values there is a range of control gain that gives good stability margins. As the unstable pole increases the control gain range reduces and becomes infeasible to obtain good stability margins for unstable poles in excess of 10 rad/s.

However, there could be a possibility of enhancing the instability level that can be handled by introducing a lead compensator in the inner-most loop which is explored in the subsequent section.

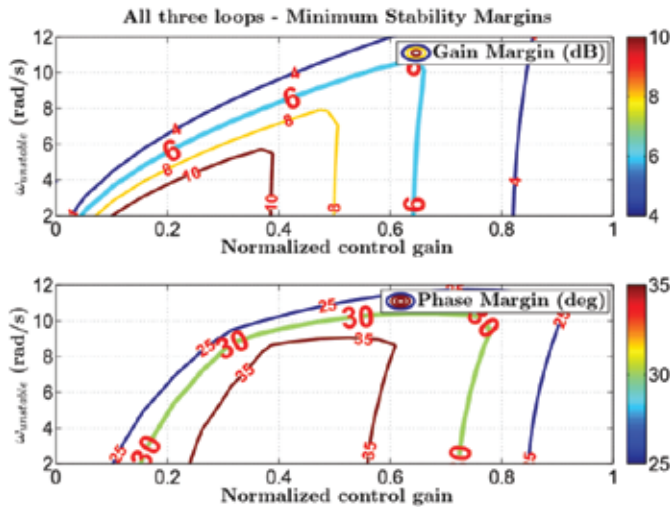


Figure 6. Stability margins - with gain iterations.

3.3 Iterative Approach - Addition of Lead Compensator

In order to enhance the maximum unstable pole that can be handled, a first order lead compensator is augmented to the autopilot design. The three autopilot gains are iterated in ranges satisfying Routh’s stability criterion. In addition to this, the location of lead compensator zero and pole are also iterated. For every combination of three-loop autopilot gains satisfying Routh’s stability criterion, the location of pole and zero are iterated for the lead compensator shown in Eqn (18)

and is cascaded in the inner-most loop.

$$LeadC = \frac{s/\omega_{num} + 1}{s/\omega_{den} + 1} \tag{18}$$

The compensator parameters iterated are marked in red in Eqn (18). For a given level of unstable pole with the iterated gains and compensators, the stability margins are evaluated. The plant perturbations on control effectiveness are also considered while evaluating the stability margins. The maximum unstable pole with which the relative stability requirements are satisfied for any combination of three-loop gains and compensator poles and zeros is obtained.

It is seen that with the actuator considered (Bandwidth = 25 Hz, Damping ratio = 0.6), for all the combinations of three-loop autopilot gains and lead compensator parameters the maximum unstable pole which could give a relative stability of Gain Margin > 6 dB, Phase Margin > 30 deg is 12 rad/s. Figure 7 shows the variation of stability margins (minimum among all the three loops) as a function of control gain as the unstable pole increases. At lower unstable pole values there is a range of control gain that gives good stability margins. As the unstable pole increases the control gain range reduces and becomes infeasible to obtain good stability margins for unstable poles in excess of 12 rad/s.

The first order lead compensator did not seem to significantly improve the maximum unstable pole that can be catered for. From the past experience of autopilot designs it is seen that the gain margin shortage is more common compared to the phase margin. Hence a unique application of lead compensator design is adopted near the phase crossover frequency to increase the phase crossover frequency and hence increase the Gain margin owing to the natural attenuation of the Bode magnitude curve. This is contrary to the conventional approach where the lead compensator is designed near the gain crossover frequency for better phase margin.

A second order lead compensator design is considered to address this aspect as follows. The second order lead compensator is chosen to locally increase the magnitude

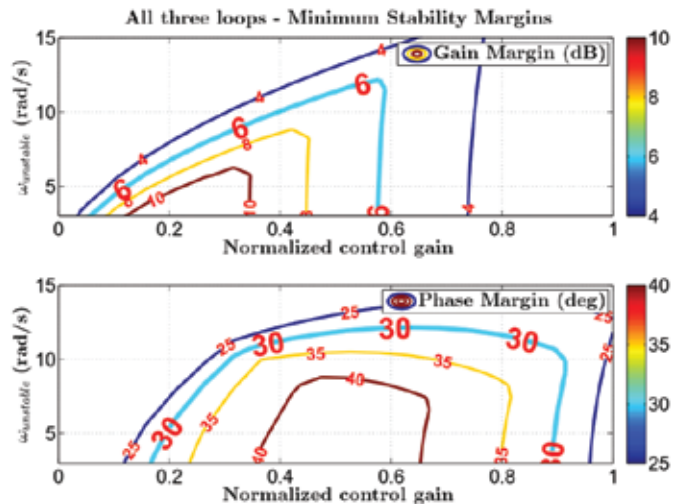


Figure 7. Stability margins - with gain and lead compensator iterations.

attenuation near the phase crossover frequency by choosing under-damped zeros, which increase the Gain margin. The natural frequency of the lead compensator pole is limited by update rate of the autopilot digital implementation on-board the interceptor.

The three autopilot gains are iterated in ranges satisfying Routh’s stability criterion. In addition to this, the location of lead compensator zeros and poles are also iterated. For every combination of three-loop autopilot gains satisfying Routh’s stability criterion, the location of poles and zeros and the damping ratio of zeros are iterated for a second order lead compensator shown in Eqn (19) and is cascaded in the inner-most loop.

$$LeadC = \frac{s^2 / \frac{\omega_{num}^2}{\omega_{den}^2} + 2\zeta_{num} / \omega_{num} s + 1}{s^2 / \frac{\omega_{den}^2}{\omega_{den}^2} + 2\zeta_{den} / \omega_{den} s + 1} \quad (19)$$

The compensator parameters iterated are marked in red in Eqn (19). The damping ratio of poles does not contribute much towards the stability margins, hence is not iterated and is chosen as critically damped (which was found to be best). For a given level of unstable pole with the iterated gains and compensators, the stability margins are evaluated. The plant perturbations on control effectiveness are also considered while evaluating the stability margins. The maximum unstable pole with which the relative stability requirements are satisfied for any combination of three-loop gains and compensator poles and zeros is obtained.

It is seen that with the actuator considered (Bandwidth = 25 Hz, Damping ratio = 0.6), for all the combinations of three-loop autopilot gains and second order lead compensator parameters the maximum unstable pole which could give a relative stability of Gain Margin > 6 dB, Phase Margin > 30 deg is 16 rad/s. Figure 8 shows the variation of stability margins (minimum among all the three loops) as a function of control gain as the unstable pole increases. At lower unstable pole values there is a range of control gain that gives good stability margin. As the unstable pole increases the control gain range reduces and becomes infeasible to obtain good stability margins for unstable poles in excess of 16 rad/s. For plant instabilities in excess of 16 rad/s, relative stability requirements cannot be guaranteed.

The lifting surface is moved forward by approximately 2.5D in order to increase the unstable pole from 5 rad/s to 16 rad/s. As the unstable pole handling capability increases, the lifting surface location can be moved forward which in turn improves the interceptor agility (time constant) during the homing phase.

4. OBSERVATION AND ANALYSIS

It is worthwhile analysing the reasons for this observation with the help of Bode characteristics. For the sake of analysis, let us first consider a comparison of Bode diagrams for a stable and unstable plant as shown in Fig. 9. For a stable open loop plant, the relative stability can be enhanced by arbitrarily reducing the gain crossover frequency using simple gain adjustment. A lower gain crossover frequency takes advantage of better phase characteristics at that frequency and better

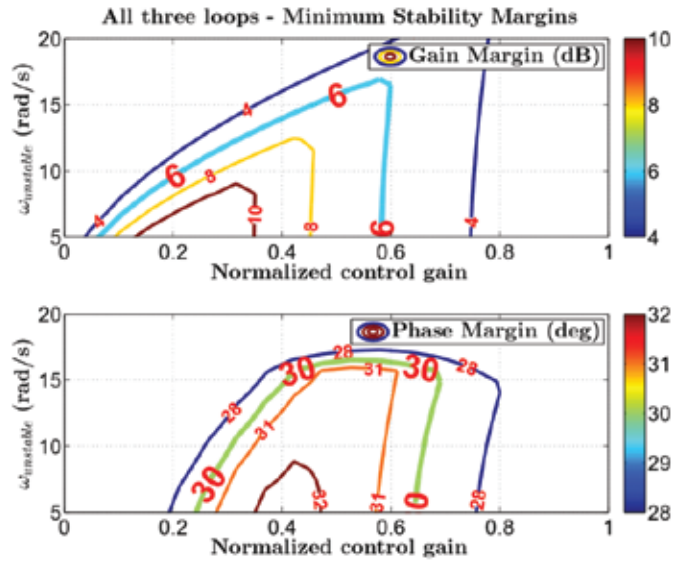


Figure 8. Stability margins - with gain and second order lead compensator iterations.

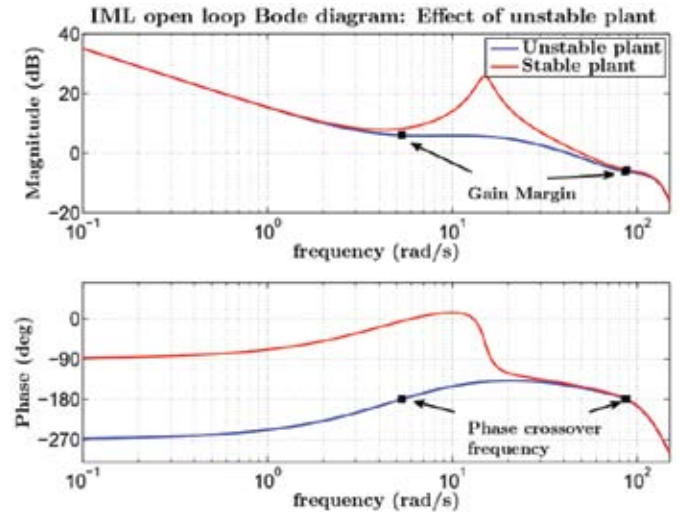


Figure 9. Inner-most loop open Bode diagram: Effect of unstable plant.

magnitude attenuation at the phase crossover frequency, which ensures good relative stability at the cost of autopilot bandwidth though.

However, the unstable plant leads to two phase crossover frequencies to satisfy Nyquist stability criterion; hence needs to ensure gain margins at both the frequencies. At the lower phase crossover frequency the unstable plant shows a significant reduction in magnitude compared to an underdamped stable plant, which makes ensuring gain margin difficult. This puts a minimum limit on gain crossover frequency below which ensuring gain margin at lower phase crossover frequency becomes impossible. Meanwhile, at the higher phase crossover frequency actuator bandwidth degrades the phase characteristics. This puts an upper limit on the gain crossover frequency above which ensuring gain margin at higher phase crossover frequency becomes difficult.

Though it may appear as if the phase crossover frequency can be increased by arbitrarily increasing the lead compensator

pole for ensuring better gain margin, the high frequency amplification associated with a lead compensator makes ensuring gain margin difficult as demonstrated in Fig. 10.

Thus it is seen that there are lower and upper limits on gain crossover frequencies for ensuring good stability margins for an unstable plant with a given actuator. In other words, with a given actuator there is a maximum unstable pole above which there is no feasible gain crossover frequency possible that ensures good stability margins. As stated earlier, through simulations it is brought out that for any combination of three-loop autopilot gains and locations of compensator poles and zeros, the maximum unstable pole for which stability margins can be guaranteed is seen to be 16 rad/s. It is also seen that the gain crossover frequency must be at least 2 - 3 times the unstable pole location of the plant to ensure good relative stability. Likewise, the actuator bandwidth should be at least 4 - 5 times the gain crossover frequency.

It should be noted that the design carried out in this paper does not consider the effect of flexible dynamics. Though the bending mode frequencies due to flexibility are in general sufficiently higher compared to the gain and phase crossover frequencies, it will have a degrading effect on the gain margin. To recover this degradation the gain crossover frequency must be further reduced. This affects the maximum unstable pole that can be handled by the control design.

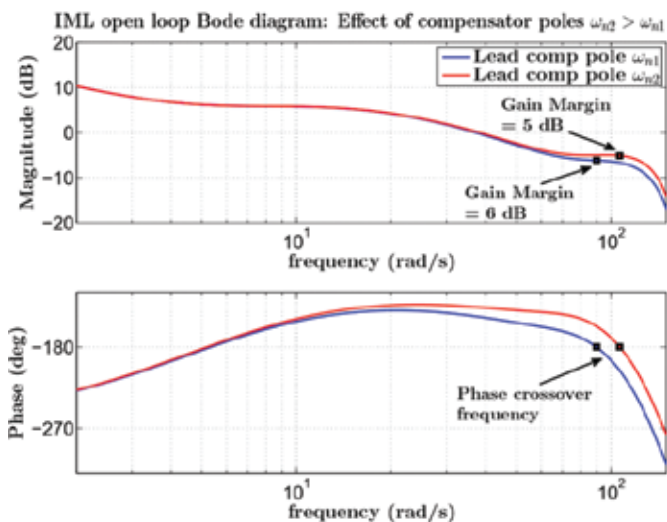


Figure 10. Inner-most loop open Bode diagram: Effect of compensator pole location.

5. CONCLUSIONS

The limitations of lax autopilot in controlling a statically unstable interceptor with a given actuator is derived. The maximum unstable pole that can be catered for with a given actuator has a strong bearing on the aerodynamic design of the interceptor. The aerodynamic maximum lax trim requirement puts a bound on the location of aerodynamic lifting surface along the length of the interceptor. A method for obtaining the optimum choice of wing location within these bounds is established based on the maximum aerodynamic instability level control design can handle. The choice of wing location using this method ensures minimum static margin during homing phase of the interceptor leading to good speed of

response. The choice of aerodynamic lifting surface location from the control design perspective is the first of its kind work to the best of author's knowledge.

REFERENCES

1. Astrom, K. Limitations on control system performance. *European J. Control.* 2000, **6**(1), 2–20. doi: 10.1016/S0947-3580(00)70906-X
2. Nesline, F. W. & Nesline, M. L. How autopilot requirements constrain the aerodynamic design of Homing missiles. *In American Control Conference*, 1984, 716–730. doi:10.23919/ACC.1984.4788471
3. Zarchan, P. Tactical and strategic missile guidance. *American Institute of Aeronautics and Astronautics*, 2012, 473–567.
4. Mracek, C. & Ridgely, D. Missile Longitudinal Autopilots: Comparison of Multiple Three Loop Topologies. *In AIAA Guidance, Navigation, and Control Conference and Exhibit*. 2005. doi: 10.2514/6.2005-6380.
5. Nesline, F. W.; Wells, B. H.; & Zarchan, P. Combined optimal/classical approach to robust missile autopilot design. *J. Guidance Control.* 1981, **4**(3), 316–322. doi: 10.2514/3.56084
6. Nesline, F. & Zarchan, P. A classical look at modern control for missile autopilot design. *In Guidance and Control Conference*, 1982. doi: 10.2514/6.1982-1512
7. Defu, L.; Junfang, F.; Zaikang, Q. & Yu, M. Analysis and improvement of missile three-loop autopilots. *J. Sys. Eng. Electron.*, 2009, **20**(4), 844–851.
8. Hai-rong, C. & Yue, Z. Three-loop autopilot design and simulation. *In 2012 IEEE International Conference on Mechatronics and Automation*. 2012, 2499–2503. doi: 10.1109/ICMA.2012.6285739
9. Mracek, C. P. Tactical Missile Autopilots. *Springer London*, 2014, 1–7. doi: 10.1007/978-1-4471-5102-9_19-1
10. Li, K.; Yang, S. & Zhao, L. Three-loop autopilot of spinning missiles. *In Proceedings of the Institution of Mechanical Engineers. Part G: J. Aerospace Eng.*, 2014, **228**(7), 1195–1201. doi: 10.1177/0954410013486870
11. Abd-elatif, M.; Qian, L.-j. & Bo, Y.-m. Optimization of three-loop missile autopilot gain under crossover frequency constraint. *Defence Technology.* 2016, **12**(1), 32–38. doi: 10.1016/j.dt.2015.08.006
12. Devaud, E.; Harcaut, J.-P. & Siguerdidjane, H. Three-axes missile autopilot design: from linear to nonlinear control strategies. *J. Guidance, Control, Dynamics*, 2001, **24**(1), 64–71. doi: 10.2514/2.4676
13. Lee, C.-H.; Jun, B.-E. & Lee, J.-I. Connections between linear and nonlinear missile autopilots via three-loop topology. *J. Guidance, Control, Dynamics*, 2016, **39**(6), 1424–1430. doi: 10.2514/1.G001565

14. Kim, J.-H. & Whang, I. H. Augmented three-loop autopilot structure based on mixed-sensitivity H_{∞} optimization. *J. Guidance, Control, Dynamics*, 2018, **41**(3), 751–756.
doi: 10.2514/1.G003119

CONTRIBUTORS

Mr Ram B. Sankar completed his BTech in Electrical and Electronics Engineering from Kerala University. He has been working as a scientist in Defence Research and Development Laboratory, Hyderabad since year 2010. His area of specialisation is guidance and control design, 6-DOF modelling and simulation of interceptors. Presently, he is pursuing MTech + PhD dual degree in Aerospace Engineering from Indian Institute of Technology Bombay.

He has carried out the simulations presented in the paper and also has written the paper.

Mr Pawan Kishore Tiwari completed his MTech in Aerospace Engineering from Indian Institute of Technology Bombay in year 2000. He has been working as a scientist in Defence Research and Development Laboratory, Hyderabad since year 2000. His area of specialisation is guidance, estimation and

control design, 6-DOF modelling and simulation of interceptors; in which he has various publications.

He has guided the research work presented in the paper.

Dr Bijnan Bandyopadhyay completed his PhD in Electrical Engineering from IIT Delhi, India in 1986. In 1987, he joined the Systems and Control Engineering group, IIT Bombay, India, as a faculty member, where he is currently a chair professor. He is a Fellow of the Indian National Academy of Engineering, National Academy of Sciences, and the Indian Academy of Sciences. His research interests include the areas of multi-rate output feedback based discrete-time sliding mode control, event-triggered sliding mode control, and nuclear reactor control. He has 400 publications which include monographs, book chapters, journal articles, and conference papers.

He has acted as an advisor to the research work presented in the paper.

Dr Hemendra Arya completed his PhD in Aerospace Engineering from Indian Institute of Technology Bombay. Presently, he is working as a faculty in Aerospace Engineering department in Indian Institute of Technology Bombay. His area of specialisation is Micro Aerial Vehicles and Hardware-in-loop simulation; in which he has various publications.

He has acted as an advisor to the research work presented in the paper.